Ancient helium and tungsten isotopic signatures preserved in mantle domains least modified by crustal recycling

M G Jackson, Janne Blichert-Toft, S A Halldórsson, A Mundl-Petermeier, M. Bizimis, M.D. Kurz, A A Price, S Harðardóttir, L N Willhite, K Breddam, et al.

Classification: PHYSICAL SCIENCES **(**Earth, Atmospheric, and Planetary Sciences)

Ancient helium and tungsten isotopic signatures preserved in mantle domains least modified by crustal recycling

M.G. Jackson[1*], J. Blichert-Toft[2‡], S.A. Halldórsson[3‡], A. Mundl-Petermeier[4], M. Bizimis[5], M.D. Kurz[6], A.A. Price[1] , S. Harðardóttir[3], L.N. Willhite[1,7], K. Breddam[8], T.W. Becker[9], R.A. Fischer[10]

[1]Department of Earth Science, University of California, Santa Barbara, 93106, USA (*corresponding author: jackson@geol.ucsb.edu)
[2]Laboratoire de Géologie de Lyon, Ecole Normale Supérieure de Lyon, CNRS, and Université de Lyon, France
[3]NordVulk, Institute of Earth Sciences, University of Iceland, Reykjavík, Iceland
[4]Department of Lithospheric Research, University of Vienna, Vienna, Austria
[5]School of the Earth, Ocean and Environment, University of South Carolina, Columbia, South Carolina, USA
[6]Department of Marine Chemistry, Woods Hole Oceanographic Institution, Woods Hole, Massachusetts, USA
[7]Department of Geology, University of Maryland, College Park, USA
[8]Danish Health Authority, Copenhagen, Denmark
[9]Institute for Geophysics and Department of Geological Sciences, The Jackson School of Geosciences, University of Texas at Austin, Austin, TX, USA
[10]Department of Earth & Planetary Sciences, Harvard University, Cambridge, MA, USA

‡Authors made equal contributions.

Abstract. Rare high-$^{3}He/^{4}He$ signatures in ocean island basalts (OIB) erupted at volcanic hotspots derive from deep-seated domains preserved in Earth's interior. Only high-$^{3}He/^{4}He$ OIB exhibit anomalous-^{182}W—an isotopic signature inherited during the earliest history of the Earth—supporting an ancient origin of high-$^{3}He/^{4}He$. However, it is not understood why some OIB host anomalous-^{182}W while others do not. We provide new geochemical data for the highest-$^{3}He/^{4}He$ lavas from Iceland (up to 42.9 times atmospheric) with anomalous-^{182}W, and examine how Sr-Nd-Hf-Pb isotopic variations—useful for tracing subducted, recycled crust—relate to high-$^{3}He/^{4}He$ and anomalous-^{182}W. These data, together with data on global OIB, show that the highest-$^{3}He/^{4}He$ and the largest magnitude ^{182}W anomalies are found only in geochemically depleted mantle domains—with high-$^{143}Nd/^{144}Nd$ and low-$^{206}Pb/^{204}Pb$—lacking strong signatures of recycled materials. In contrast, OIB with the strongest signatures associated with recycled materials have low-$^{3}He/^{4}He$ and lack anomalous-^{182}W. These observations provide important clues regarding the survival of the ancient He and W signatures in Earth's mantle. We show that high-$^{3}He/^{4}He$ mantle domains with anomalous-^{182}W have low W and ^{4}He concentrations compared to recycled materials and are therefore highly susceptible to being overprinted with low-$^{3}He/^{4}He$ and normal (not anomalous) ^{182}W characteristic of subducted crust. Thus, high-$^{3}He/^{4}He$ and anomalous-^{182}W are preserved exclusively in mantle domains least modified by recycled crust. This model places the long-term preservation of ancient high-$^{3}He/^{4}He$ and anomalous-^{182}W in the geodynamic context of crustal subduction and recycling, and informs on survival of other early-formed heterogeneities in Earth's interior.

Keywords: Mantle geochemistry, hotspot volcanism, ^{182}W, $^{3}He/^{4}He$, Hadean, core, mantle

Significance Statement. The recent discovery of anomalous-^{182}W signatures in modern, plume-derived hotspot lavas provides evidence for survival of domains in Earth's interior since the early Hadean. Critically, only lavas with ancient, high-$^{3}He/^{4}He$ signatures preserve anomalous-^{182}W signatures. However, it is still not known why only high-$^{3}He/^{4}He$ lavas have anomalous-^{182}W, while other hotspot lavas do not. Here we show that only hotspot lavas lacking strong recycled crust signatures exhibit high-$^{3}He/^{4}He$ and anomalous-^{182}W. This observation is explained by subduction of W- and ^{4}He-rich crust that has low-$^{3}He/^{4}He$ and normal-^{182}W: following subduction, the crust masks high-$^{3}He/^{4}He$ and anomalous-^{182}W signatures characteristic of ancient mantle domains. Thus, our model links destruction of Hadean geochemical signatures with the well-established geodynamic process of plate subduction and crustal recycling.

Introduction

Plate tectonic motions deliver oceanic and continental crust into the mantle at subduction zones. Following residence times of ~2 Ga, subducted crustal material is returned to the shallow mantle in buoyantly upwelling conduits of hot mantle material, known as mantle plumes, where they are partially melted and erupted as OIB at volcanic hotspots (1-3). Recycled materials contribute to a variety of geochemically-distinct mantle components often referred to as EM1 (enriched mantle I), EM2 (enriched mantle II), and HIMU (high 'μ' or high $^{238}U/^{204}Pb$) (1-3). While there is debate surrounding the exact nature of the recycled protoliths responsible for these mantle endmembers (4-7), they are likely generated by input of shallow geochemical reservoirs into the deep Earth. The three mantle components have $^{87}Sr/^{86}Sr$, $^{143}Nd/^{144}Nd$, $^{176}Hf/^{177}Hf$, and $^{206}Pb/^{204}Pb$ distinct from the depleted mantle (DM) sampled by basalts erupted at mid-ocean ridges (MORB). In three-dimensional Sr-Nd-Pb isotopic space, these four geochemical endmembers can be used to define the apices of a tetrahedron (8) (Figure 1), and have low $^{3}He/^{4}He$, similar to, or lower than, MORB (8 ± 2 Ra, ratio to atmosphere) (9). An additional mantle component is found internal to the other four and, like DM, is characterized by geochemically depleted compositions that relate to long-term crustal extraction from the mantle, which changes the parent-daughter ratios that govern key radiogenic isotopic systems, resulting in high $^{143}Nd/^{144}Nd$ and $^{176}Hf/^{177}Hf$ coupled with low $^{87}Sr/^{86}Sr$ and $^{206}Pb/^{204}Pb$. Existing long-lived radiogenic isotopic data show that this fifth component is geochemically depleted (8,10), and has been variously referred to as FOZO (Focus Zone (8)), PHEM (Primordial Helium Mantle (11)), or C (Common (12)). In contrast to DM, this geochemically depleted mantle composition was argued to exhibit elevated $^{3}He/^{4}He$ (8), signaling the preservation of an ancient reservoir in the deep Earth (13).

Recent discoveries employing the short-lived ^{182}Hf-^{182}W isotopic systematics have demonstrated the presence of anomalous, negative $\mu^{182}W$ (where μ is the deviation of $^{182}W/^{184}W$ from the terrestrial standard in parts per million) in modern OIB (14-17), and the anomalies are found uniquely in lavas with high $^{3}He/^{4}He$ (14-16). ^{182}W anomalies were generated only while the parent nuclide ($^{182}Hf \rightarrow {}^{182}W+2\beta^-$, $t_{1/2}$ = 8.9 Ma) was extant (i.e., < 60 Ma following Solar System formation), so the observation of anomalous ^{182}W signals in the modern mantle implies that these signatures have been preserved in the Earth since the early Hadean. This is consistent with the discovery of heterogeneous ^{129}Xe and ^{142}Nd—

which are products of the short-lived isotopes ^{129}I and ^{146}Sm, respectively, extant only in the Hadean (18,19)—in the modern mantle, further supporting the observation of chemical heterogeneities preserved in the Earth's interior since the Hadean.

An important recent observation is that ^{182}W and ^{3}He/^{4}He data from oceanic basalts define a negatively sloping array, with anomalous ^{182}W signatures in OIB uniquely associated with lavas that exhibit high ^{3}He/^{4}He (14-16). This fundamental advance relates primordial high ^{3}He/^{4}He with an early-formed isotopic heterogeneity. However, several outstanding questions regarding ^{182}W systematics in the modern mantle remain: 1) What is the mechanism responsible for the unique association of anomalous μ^{182}W with high-^{3}He/^{4}He hotspots lavas, and why do low-^{3}He/^{4}He lavas lack ^{182}W anomalies? 2) Do the geodynamic processes of subduction and recycling impact the ^{182}W-^{3}He/^{4}He mantle array? 3) Do ^{182}W systematics exhibit relationships with isotopic tracers (i.e., Sr-Nd-Pb) sensitive to crustal subduction and recycling, or are ^{182}W systematics somehow insensitive to these geodynamic processes such that Sr-Nd-Pb isotope systematics are decoupled from ^{182}W?

In order to address these outstanding questions, we provide a new large geochemical dataset on high-^{3}He/^{4}He lavas from the Iceland hotspot, and examine the data in the context of new global OIB datasets combining He, Sr, Nd, Hf, and Pb isotopes with W isotopes. The data and analysis provide new insights into the mechanisms for preservation of anomalous ^{182}W and high-^{3}He/^{4}He signatures in the mantle.

Results

We present new He-Sr-Nd-Hf-Pb-W isotopic data (see Materials and Methods) on a suite of 28 basalt samples from all Icelandic localities known to have high ^{3}He/^{4}He (> 25 Ra): mid-Miocene lavas from northwest Iceland (Vestfirðir), as well as Neovolcanic zone lavas from the Eastern Rift Zone (ERZ), the South Iceland Volcanic Zone (SIVZ), and Vaðalda shield volcano in the Northern Rift Zone (NRZ) (20-22) (SI Appendix, Figure S1, Datasets S1, S2, and S3). These data are presented together with published data (23) from ~60 Ma Baffin Island and West Greenland (BIWG) flood basalt lavas, an additional high-^{3}He/^{4}He (up to 50 Ra (23-26)) locality on the Iceland hotspot track. He, Pb, and W isotopic data on a small subset (*N* = 8, 9, and 10, respectively) of the Iceland samples examined here (14,15), as well as

$^{3}He/^{4}He$ data on a different subset of ten samples (20,22), were published previously. The dataset presented here includes new $^{87}Sr/^{86}Sr$ and $^{143}Nd/^{144}Nd$ for all 28 samples, and new $^{176}Hf/^{177}Hf$ and Pb isotopic measurements for 27 and 19 samples, respectively. We also present new $^{3}He/^{4}He$ measurements by coupled vacuum crushing and fusion of olivine and clinopyroxene crystals on ten samples (including one sample with the highest $^{3}He/^{4}He$ in the dataset, 42.9 Ra; Figure 2; SI Appendix, Figure S2), and new $^{3}He/^{4}He$ measurements by fusion on the same powders from nine samples with previously published $^{3}He/^{4}He$ by crushing (15). We present a new W isotopic measurement on the highest $^{3}He/^{4}He$ ERZ lava, complementing 10 prior measurements made on this suite of 28 samples (15) (additional ^{182}W analyses on a different suite of 6 Icelandic lavas are also available (15)). Additionally, we present new major and trace element data for all of the mid-Miocene Vestfirðir lavas and a subset of the Neovolcanic zone lavas (SI Appendix, Figure S3). The new and published data on the 28 samples of this study represent the first full geochemical characterization of all known high-$^{3}He/^{4}He$ localities in Iceland.

The new Iceland dataset, combined with Sr-Nd-Pb isotope data from the literature, expands the number of OIB samples characterized for both ^{182}W (14-17) and Sr-Nd-Pb isotopic compositions by nearly 60% (SI Appendix, Dataset S4). This augmented dataset allows examination of relationships between Sr-Nd-Pb isotopes, traditionally used to detect signatures of crustal recycling, and $^{3}He/^{4}He$ and ^{182}W, which can trace early-formed reservoirs in the Earth.

In Figure 2 and SI Appendix Figure S4, the He-Sr-Nd-Hf-Pb isotopic compositions for most (~75%) of the Iceland lavas with $^{3}He/^{4}He > 21$ Ra are presented here for the first time and show that the highest $^{3}He/^{4}He$ lavas sample four high-$^{3}He/^{4}He$ components with distinct Sr-Nd-Hf-Pb isotopic compositions. The Vestfirðir (up to 42.9 Ra) and Vaðalda (33.6 Ra) lavas are similar geochemically and are grouped together. The Vaðalda lava shows the recent (Pleistocene) reappearance of a geochemical component not known in Iceland since the mid-Miocene (Figure 2; SI Appendix, Figure S4). The ERZ lavas host a second Iceland high-$^{3}He/^{4}He$ component (25.9 Ra; SI Appendix, Dataset S1) with Sr-Nd-Hf isotopic ratios more geochemically depleted than Vestfirðir and Vaðalda lavas. The SIVZ lavas represent a third Iceland high-$^{3}He/^{4}He$ component (25.7 to 26.2 Ra (20); SI Appendix, Dataset S1) with $^{206}Pb/^{204}Pb$ higher than the other two components. A fourth high-$^{3}He/^{4}He$ Iceland component is evident in previously published geochemical datasets from BIWG, which have $^{3}He/^{4}He$ up to 50 Ra, the highest known

terrestrial mantle-derived $^{3}He/^{4}He$ (23-26)): after applying major and trace element filters for continental crust assimilation (23), the Baffin Island lavas exhibit the lowest $^{206}Pb/^{204}Pb$ identified along the Iceland hotspot track (Figure 2).

The four geochemically-distinct high-$^{3}He/^{4}He$ Iceland components are clearly resolved in Sr-Nd-Hf-Pb isotope space (Figure 2; SI Appendix, Figure S4), and the range in $^{206}Pb/^{204}Pb$ across the four Iceland high-$^{3}He/^{4}He$ components found at five geographic locations—Vestfirðir/Vaðalda, ERZ, SIVZ, and BIWG—spans a remarkable ~40% of the total variability found in global OIB (Figure 2; SI Appendix, Figure S4). The wide range of Sr-Nd-Hf-Pb isotopic compositions in Icelandic, and global (including Hawaii, Samoa, and Galapagos), high-$^{3}He/^{4}He$ (> 25 Ra) lavas is notable. Nonetheless, high-$^{3}He/^{4}He$ lavas globally exhibit geochemically depleted Sr-Nd-Hf isotopic signatures and relatively unradiogenic $^{206}Pb/^{204}Pb$ compositions ($^{206}Pb/^{204}Pb$ < 19.5) (Figure 2; SI Appendix, Figure S4), where the chondritic reference frame for $^{143}Nd/^{144}Nd$ and $^{176}Hf/^{177}Hf$ serves as reference point for geochemical depletion: geochemically depleted lavas have $^{143}Nd/^{144}Nd$ and $^{176}Hf/^{177}Hf$ ratios higher than chondrites (i.e., as shown for $^{143}Nd/^{144}Nd$ in Figure 3). Complementing negative $\mu^{182}W$ anomalies observed in high-$^{3}He/^{4}He$ hotspot lavas globally (14-16), Vestfirðir and SIVZ lavas have negative $\mu^{182}W$ anomalies (15), and we further report here another resolvable negative $\mu^{182}W$ anomaly (-10.0 ± 3.8) in the highest $^{3}He/^{4}He$ ERZ lava (SI Appendix, Dataset S2). However, recently published ^{182}W measurements of the high-$^{3}He/^{4}He$ BIWG lavas do not reveal $\mu^{182}W$ anomalies (15), which is discussed below.

In Figure 1, Sr-Nd-Pb isotopic compositions of the lavas that define the four Iceland high-$^{3}He/^{4}He$ components, and the highest $^{3}He/^{4}He$ lavas from other hotspots, are compared with the common mantle component. This component is shown as an ellipsoid and represents the 95% confidence interval for the volume encompassing the best-fit intersections of the trendlines that were fit to OIB arrays formed by individual hotspots (27), as this component (i.e., FOZO) was originally defined by the intersection of global OIB arrays (8) (but we note that not all OIB arrays extend into the common component region). In Iceland, only the highest $^{3}He/^{4}He$ lava from the SIVZ plots within the common mantle component ellipsoid, while the highest $^{3}He/^{4}He$ ERZ, Vestfirðir, and Baffin Island lavas are shifted toward compositions more geochemically depleted (and in the case of Baffin Island, more similar to MORB) than the common mantle component. Among the other hotspots globally with $^{3}He/^{4}He$ > 25 Ra, only the

Galapagos high-$^{3}He/^{4}He$ lava (30.3 Ra) plots within the ellipsoid, while Hawaiian (32.3 Ra) and Samoan (33.4 Ra) high-$^{3}He/^{4}He$ lavas do not (Figure 1). In summary, most of the highest $^{3}He/^{4}He$ OIB globally are not necessarily associated with the common mantle component in Sr-Nd-Pb isotopic space, as previously defined. Due to this isotopic variability, we do not refer to the high-$^{3}He/^{4}He$ mantle domain with anomalous ^{182}W as FOZO, C, or PHEM, all of which share depleted characteristics.

The geochemically depleted high-$^{3}He/^{4}He$ mantle is most clearly distinguished from the geochemically depleted DM by having high $^{3}He/^{4}He$ and anomalous ^{182}W. However, due to extreme geochemical depletion in some high-$^{3}He/^{4}He$ lavas (in particular the BIWG lavas), we are not able to specify which mantle domain, DM or high-$^{3}He/^{4}He$, extends to more geochemically depleted compositions. Nonetheless, we show for the first time that only geochemically depleted mantle domains have the largest magnitude $\mu^{182}W$ anomalies. The association of anomalous $\mu^{182}W$ with geochemical depleted mantle (i.e., superchondritic $^{143}Nd/^{144}Nd$ and $^{176}Hf/^{177}Hf$) provides key insights into processes responsible for the preservation, and destruction, of ^{182}W anomalies in Earth's interior.

Discussion

Influence of recycled crust on high-$^{3}He/^{4}He$ and anomalous ^{182}W signatures in the mantle. An important issue in chemical geodynamics is how short-lived radiogenic isotopic signatures generated in the Hadean Earth—^{182}W, ^{142}Nd, and ^{129}Xe—have survived in the convecting mantle to be sampled by modern OIB (16-19). The presence of high $^{3}He/^{4}He$ and anomalous ^{182}W in Iceland hotspot lavas require a mechanism for preserving these ancient signatures in the OIB mantle. We argue that the survival of high-$^{3}He/^{4}He$ and anomalous ^{182}W signatures in the convecting mantle will depend on whether anomalous ^{182}W and high-$^{3}He/^{4}He$ mantle domains mix with W- and ^{4}He-rich recycled materials, or with DM, which also has low $^{3}He/^{4}He$ and normal ^{182}W. Compared to domains with anomalous ^{182}W and high $^{3}He/^{4}He$, the mantle endmembers sampling recycled materials—EM1, EM2, and HIMU—lack anomalous $\mu^{182}W$. Subducted oceanic and continental crust have high W concentrations and will not necessarily host anomalous $\mu^{182}W$ (if derived from reservoirs that formed after the early Hadean), and they will evolve high ^{4}He concentrations and low $^{3}He/^{4}He$ over time (due to having higher U and Th concentrations and to loss of He during subduction) (see SI Appendix, Datasets S5 and S6 for data sources). Thus, one hypothesis

is that subducted crust can overprint high-$^{3}He/^{4}He$ and anomalous $\mu^{182}W$ signatures with low $^{3}He/^{4}He$ and normal $\mu^{182}W$, explaining why mantle domains similar to EM1, EM2, and HIMU have low $^{3}He/^{4}He$ and lack anomalous $\mu^{182}W$, while domains with high $^{3}He/^{4}He$ and anomalous $\mu^{182}W$ do not extend to extreme EM (low $^{143}Nd/^{144}Nd$) or HIMU (high $^{143}Nd/^{144}Nd$ and high $^{206}Pb/^{204}Pb$) compositions that reflect large contributions form W- and ^{4}He-rich recycled materials (Figure 3; SI Appendix, Figure S5).

The addition of variable quantities of subducted materials to mantle domains with anomalous ^{182}W is a potential mechanism to explain variability in the magnitude of recently discovered ^{182}W anomalies in modern hotspot lavas. Before the discovery of ^{182}W anomalies in the present-day mantle, subduction and recycling of W-rich crust was considered as a possible mechanism to explain the complete absence of detectable core-derived ^{182}W anomalies in the Earth's mantle (28,29). However, the discovery of ^{182}W variability in the modern mantle indicates that ^{182}W heterogeneity has not been entirely overprinted with subducted crust. Thus, we explore a more nuanced version of this early model to gain new insights into the coupled ^{182}W-$^{3}He/^{4}He$ systematics of the mantle. We quantitatively examine the influence of recycled crust and DM on mantle domains that host anomalous $\mu^{182}W$ and high-$^{3}He/^{4}He$ compositions (Figure 4).

In $\mu^{182}W$ versus $^{3}He/^{4}He$ space, the data form a negatively-sloping array that is composed of subtrends formed by different hotspots (14-16), and the strength of the overall global trend is supported by a high correlation (Spearman rank coefficient $r_s = -0.67 \pm 0.07$) (Figure 4). Assuming an average age for recycled crust of 2 Ga (an age consistent with the slope of the Northern Hemisphere Reference Line (NHRL) in Pb isotopic space (30)), we show that mixing ancient subducted oceanic and continental crust with high-$^{3}He/^{4}He$ mantle sources of OIB with anomalous $\mu^{182}W$ forms mixing trends with negatively sloping arrays that describe the coupled $\mu^{182}W$ and $^{3}He/^{4}He$ systematics of global OIB (Figure 4).

Absolute He and W concentrations in the mantle are not well constrained, but the concentration contrast between high-$^{3}He/^{4}He$ mantle domains and subducted materials can be inferred to construct the mixing models in Figure 4. All W and He isotopic compositions and mantle source concentrations for the model in Figure 4 are provided in SI Appendix, Dataset S5. Compared to the high-$^{3}He/^{4}He$ mantle, oceanic and continental crust is expected to have high concentrations of W (0.12 and 1.9 ppm, respectively) (31, 32) and ^{4}He, the latter due to the decay of Th and U (which are elevated in oceanic and

continental crust relative to the high-$^{3}He/^{4}He$ mantle). High-$^{3}He/^{4}He$ lavas with anomalous ^{182}W from Hawaii (Loihi) provide a window into the W concentration of the high-$^{3}He/^{4}He$ mantle, which is calculated by melt models to have W concentrations (0.011 ± 0.005 ppm W (33)) that are approximately 11 and 170 times lower than subducted oceanic and continental crust, respectively. The mantle sources of high-$^{3}He/^{4}He$ lavas have He concentrations (34) that are estimated to be approximately >9 and >80 times lower than subducted oceanic and continental crust, respectively (see SI Appendix, Dataset S5). Taking these W and He concentrations as representative of the high-$^{3}He/^{4}He$ mantle with anomalous ^{182}W, subducted crust can overwhelm the W and He budgets of high-$^{3}He/^{4}He$ mantle domains, overprinting them with low $^{3}He/^{4}He$ and normal $\mu^{182}W$, and thus generating the negatively sloping global OIB array in Figure 4. Finally, adding DM—which likewise has low $^{3}He/^{4}He$ (8 Ra) and normal $\mu^{182}W$—to the high-$^{3}He/^{4}He$ mantle also generates a negatively sloping array that follows the slope of the OIB field in $\mu^{182}W$-$^{3}He/^{4}He$ space (Figure 4; DM He (34) and W (33) concentrations are provided in SI Appendix, Dataset S5). The takeaway message is that anomalous ^{182}W and high $^{3}He/^{4}He$ in plume-fed hotspots, such as Iceland, are derived from mantle domains in which these ancient signatures are not completely overprinted by recycled materials, or mixing with DM.

This model for overprinting of the high-$^{3}He/^{4}He$ mantle by mixing with recycled oceanic and continental crust is also consistent with the generation of low $^{3}He/^{4}He$ and normal ^{182}W observed in OIB endmembers EM1, EM2, and HIMU (Figure 4, SI Appendix, text, Dataset S5). Other recycled materials could overprint domains with high $^{3}He/^{4}He$ and anomalous ^{182}W, but such materials would also need to be 1) relatively enriched in W (to effectively mask anomalous ^{182}W domains) and 2) degassed in He and enriched in Th and U (to generate both the high ^{4}He concentrations and low $^{3}He/^{4}He$ that are necessary to mask high-$^{3}He/^{4}He$ domains). Nonetheless, mixing ancient subducted continental and oceanic crust, as done in Figure 4, serves to illustrate how recycled materials efficiently overprint high-$^{3}He/^{4}He$ and anomalous ^{182}W domains in the mantle.

Quantifying the relationship between ^{182}W and crustal recycling. It has long been assumed that addition of recycled materials to the mantle results in mantle domains with low $^{3}He/^{4}He$ (13,35,36), which is supported by the modelling exercise in Figure 4, and the observation that mantle endmembers hosting

the strongest recycling signatures in Sr-Nd-Pb isotopic space—EM1, EM2, and HIMU—have low $^{3}He/^{4}He$ (≤ 8 Ra). However, the relationships between $\mu^{182}W$ and Sr-Nd-Pb isotopes, and the impact of subducted materials on $\mu^{182}W$ signatures in OIB, remain to be explored in detail. Armed with a dataset of Sr-Nd-Pb-W isotopes on global OIB (SI Appendix, Dataset S4), we identify clear relationships between $\mu^{182}W$ and recycled signatures in OIB (Figure 5).

Based on the modelling in Figure 4, we propose that, if mixed with a high-$^{3}He/^{4}He$ component having anomalous ^{182}W, mantle domains lacking input of recycled crust will have the most extreme negative ^{182}W anomalies, and that addition of progressively larger quantities of recycled crust will cause a reduction in the magnitude of the ^{182}W anomaly. This hypothesis is difficult to test because no single isotopic ratio is indicative of recycled materials that contribute to HIMU *and* recycled materials that contribute to EM1 and EM2: high $^{206}Pb/^{204}Pb$ can be used to identify a contribution from a HIMU component, but the $^{206}Pb/^{204}Pb$ ratio is less effective in identifying EM components; low $^{143}Nd/^{144}Nd$ and high $^{87}Sr/^{86}Sr$ ratios can be used to identify EM component contributions, but are less effective in identifying HIMU contributions. A single parameter is needed that indicates the magnitude of contribution from the various mantle endmembers. Therefore, we propose a “mantle endmember index” that draws on $^{87}Sr/^{86}Sr$, $^{143}Nd/^{144}Nd$, and $^{206}Pb/^{204}Pb$ to quantify the contribution of EM1-EM2-HIMU mantle endmember melt compositions to OIB lavas. This index allows evaluating how a fourth isotope system (e.g., $\mu^{182}W$) varies in lavas as a function of the magnitude of the contribution from any of the mantle endmembers (Figure 5). Central to this index are two assumptions: 1) Lavas sampling geochemically depleted mantle (DM)—which has low $^{206}Pb/^{204}Pb$, low $^{87}Sr/^{86}Sr$, and high $^{143}Nd/^{144}Nd$—lack a significant component of recycled materials, and 2) an increase in the contribution of recycled material results in a shift away from the depleted mantle composition in Sr-Nd-Pb isotopic space towards HIMU and EM compositions (Figure 5). Larger shifts correspond to greater recycled contributions.

This shift away from the geochemically depleted mantle (DM) can be measured as a distance ($D^{Sr\text{-}Nd\text{-}Pb}$) in three-dimensional $^{87}Sr/^{86}Sr$-$^{143}Nd/^{144}Nd$-$^{206}Pb/^{204}Pb$ space, using the following equation:

$$D^{Sr\text{-}Nd\text{-}Pb} = [((^{87}Sr/^{86}Sr_O - ^{87}Sr/^{86}Sr_D)/X)^2 + ((^{143}Nd/^{144}Nd_O - ^{143}Nd/^{144}Nd_D)/Y)^2 + ((^{206}Pb/^{204}Pb_O - ^{206}Pb/^{204}Pb_D)/Z)^2]^{0.5}$$

where the subscripts O and D indicate the isotopic composition of any “OIB” sample and the geochemically “depleted” reference composition, respectively; the depleted reference composition has Sr-Nd-Pb isotopes of 0.7025, 0.5132, and 17.5, respectively; X, Y, and Z represent the Sr-Nd-Pb isotopic differences between the geochemically depleted reference composition and the most extreme crustal recycling signatures in OIB considered in $^{87}Sr/^{86}Sr$ (0.7186 - 0.7025), $^{143}Nd/^{144}Nd$ (0.5132 - 0.5123), and $^{206}Pb/^{204}Pb$ (22.0 - 17.5) isotopic spaces, respectively. Higher values of $D^{Sr\text{-}Nd\text{-}Pb}$ for an OIB sample reflect a greater contribution from EM1, EM2, and/or HIMU (and therefore more recycled materials), while lower values indicate that lavas are more similar to the DM component and indicate a smaller contribution from these three mantle endmembers (and therefore less recycled material) (see right panel in Figure 5). A similar parameter for measuring distance in three-dimensional Pb isotope multispace (i.e., $D^{208/207/206Pb}$) was developed elsewhere (37) and serves as the basis for the $D^{Sr\text{-}Nd\text{-}Pb}$ parameter presented here.

Figure 5 shows $\mu^{182}W$ in OIB as a function of $D^{Sr\text{-}Nd\text{-}Pb}$ and demonstrates that all OIB data with the most extreme negative $\mu^{182}W$ have low $D^{Sr\text{-}Nd\text{-}Pb}$ values (< 0.65), consistent with the hypothesis that only lavas sampling geochemically depleted mantle domains (i.e., lacking significant recycled materials), host the most extreme negative $\mu^{182}W$ anomalies. However, many geochemically depleted lavas with low $D^{Sr\text{-}Nd\text{-}Pb}$ values lack anomalous ^{182}W, and this is accounted for by dilution of the anomalous ^{182}W by entrainment of a depleted mantle (DM) component lacking anomalous ^{182}W, which melts in the shallow mantle with the host plume, and subsequently mixes with melts of the high-$^{3}He/^{4}He$ plume component. This process is described by the binary mixing line to MORB in Figure 5. For example, the subset of lavas from Iceland with normal $\mu^{182}W$ may result from addition of a MORB component, consistent with the mixing line between high-$^{3}He/^{4}He$ mantle melts and MORB in Figure 5. While a depleted component has been suggested to be inherent to the Iceland plume (38,39), it is also possible that the plume has incorporated ambient depleted upper mantle during ascent (40), consistent with our hypothesis for reduction in the magnitude of ^{182}W anomalies in the Iceland plume by mixing with DM melts.

At higher $D^{Sr\text{-}Nd\text{-}Pb}$ values, and thus increasing fractions of recycled materials, the magnitude of the $\mu^{182}W$ anomalies diminishes in lavas at hotspots that host anomalous $\mu^{182}W$. For example, at maximum contributions of recycled materials, lavas sampling endmember EM1 (Pitcairn, $D^{Sr\text{-}Nd\text{-}Pb}$ = 0.85), EM2 (Samoa, $D^{Sr\text{-}Nd\text{-}Pb}$ = 1.44), and HIMU (Mangaia Island on the Macdonald hotspot track, $D^{Sr\text{-}Nd\text{-}Pb}$ =

0.99) all lack $\mu^{182}W$ anomalies. Critically, the magnitude of the recycled crust signature appears to modulate the magnitude of the anomalous ^{182}W signature: OIB samples with progressively higher values of $D^{Sr\text{-}Nd\text{-}Pb}$ at the Pitcairn, Samoa, and Macdonald hotspots show diminished $\mu^{182}W$ anomalies (Figure 5). In contrast, input of less recycled material (i.e., lower $D^{Sr\text{-}Nd\text{-}Pb}$) corresponds with increasingly negative $\mu^{182}W$ anomalies. For example, the single Pitcairn lava with a slightly negative $\mu^{182}W$ anomaly has the lowest $D^{Sr\text{-}Nd\text{-}Pb}$ in the sample suite and also the highest $^3He/^4He$ among Pitcairn lavas. This pattern is also reflected in Macdonald and Samoan hotspot samples, where lavas with the lowest $D^{Sr\text{-}Nd\text{-}Pb}$ also have the lowest $\mu^{182}W$ and the highest $^3He/^4He$ (Figure 5). Figure 5 further shows that the relationship between $D^{Sr\text{-}Nd\text{-}Pb}$ and $\mu^{182}W$ at these three hotspots, which sample the three canonical mantle endmembers, is consistent with binary mixing trends between the most anomalous $\mu^{182}W$ component and the recycled crust endmembers (EM1, EM2, and HIMU). The mixing trends are consistent with an increasing contribution of recycled materials being responsible for the dilution of anomalous $\mu^{182}W$ signatures (mixing model endmembers are in SI Appendix, Dataset S6). Thus, while the exact mechanism for the Hadean origin of $\mu^{182}W$ anomalies is not known (see below), it is clear that crustal subduction and recycling play a central role in modulating the expression of these anomalies in OIB. Finally, we anchor the mixing models in Figure 5 to an extreme low $\mu^{182}W$ composition (i.e., from Fernandina, Galapagos) only because this composition represents the most negative value (-22.7) in the existing OIB dataset. As the OIB $\mu^{182}W$ dataset expands in the future, we might expect highly negative $\mu^{182}W$ anomalies to be present in OIB over a range of Sr-Nd-Pb isotopic compositions and therefore over a range of $D^{Sr\text{-}Nd\text{-}Pb}$ values, just as high-$^3He/^4He$ signatures are found in lavas with heterogeneous Sr-Nd-Pb isotopic compositions and $D^{Sr\text{-}Nd\text{-}Pb}$ values (SI Appendix, Figure S5). However, like high-$^3He/^4He$ lavas, we anticipate that lavas with highly negative $\mu^{182}W$ will be limited to those with geochemically depleted isotopic compositions and low $D^{Sr\text{-}Nd\text{-}Pb}$ values, due to the masking influence of recycled materials on both high-$^3He/^4He$ and anomalous $\mu^{182}W$ signatures in the mantle.

Some hotspot localities with existing $\mu^{182}W$ data lack Sr-Nd-Pb isotopic data, and thus $D^{Sr\text{-}Nd\text{-}Pb}$ cannot be calculated. For example, Canary hotspot lavas from La Palma lack $\mu^{182}W$ anomalies (14,41,42) (SI Appendix, Dataset S4) and the lavas analyzed for $\mu^{182}W$ do not have complete Sr-Nd-Pb isotopic datasets. The lack of $\mu^{182}W$ anomalies may be consistent with contribution from a HIMU component

present in some La Palma lavas (43), which would be associated with high $D^{Sr\text{-}Nd\text{-}Pb}$ values that are linked to recycled crust that masks anomalous $\mu^{182}W$. If the strength of the global relationship between $\mu^{182}W$ and $^{3}He/^{4}He$ serves as a guide to which OIB host anomalous $\mu^{182}W$ (Figure 4), then the lack of high-$^{3}He/^{4}He$ at the Canaries (the highest-$^{3}He/^{4}He$ value is 9.7 Ra (44)) is consistent with the absence of anomalous ^{182}W signatures.

The presence of extreme negative $\mu^{182}W$ only in global OIB with $^{143}Nd/^{144}Nd > 0.5127$ (Figure 3) is explained by the fact that lavas with low $^{143}Nd/^{144}Nd$ values (< 0.5127) may be impacted by subducted continental crust (as suggested for the low $^{143}Nd/^{144}Nd$ in EM1 (6) and EM2 (36 lavas), a mechanism that both reduces $^{143}Nd/^{144}Nd$ and masks anomalous $\mu^{182}W$. At the more geochemically depleted end of the spectrum, where additional $\mu^{182}W$ anomalies may be found in the future, there is currently a lack of OIB with existing $\mu^{182}W$ analyses. Figure 5 calls particular attention to the lack of data among the most geochemically depleted OIB, as there is a total absence of ^{182}W-characterized lavas with $D^{Sr\text{-}Nd\text{-}Pb} < 0.25$. Given their geochemically depleted isotopic signatures (with $^{143}Nd/^{144}Nd$ to ~0.5131) (16,24,25), and their extreme high $^{3}He/^{4}He$ (up to 50 Ra) (23-26), the proto-Iceland plume BIWG continental flood basalts (CFB) offer an important opportunity in this regard, and is discussed below. For example, the least crustally-contaminated lavas among the Baffin Island suite (23) have $D^{Sr\text{-}Nd\text{-}Pb}$ ranging from 0.11 to 0.17. However, continental crust contamination represents a challenge for identifying mantle source $\mu^{182}W$ signatures in these lavas.

The case of the BIWG high-$^{3}He/^{4}He$ CFB. While all high-$^{3}He/^{4}He$ OIB have anomalous $\mu^{182}W$ (14-16), the high-$^{3}He/^{4}He$ West Greenland CFB lavas lack resolvable $\mu^{182}W$ anomalies in lavas with $^{3}He/^{4}He$ up to 48 Ra (15). This contrasts with results from an earlier study, which reported positive $\mu^{182}W$ (up to $\mu^{182}W$ = +48.4) for lavas from Baffin Island and the Ontong Java Plateau (OJP) ($\mu^{182}W$ = +23.9) (45). However, $\mu^{182}W$ anomalies were not identified in analyses of OJP lavas in other studies (41,46). Until the positive $\mu^{182}W$ for OJP and Baffin Island (15) are replicated, we will not include them in further discussion in this paper. In Figures 3 and 5 (and SI Appendix, Figure S5), we show OJP as lacking anomalous ^{182}W (41,46). Additionally, we rely on recent ^{182}W analyses from West Greenland (15) to constrain the composition of the proto-Iceland plume.

394 The absence of negative $\mu^{182}W$ anomalies in the West Greenland picrites might reflect an
395 absence of anomalous $\mu^{182}W$ in the mantle source (15). Alternatively, it could result from shallow level
396 continental crust contamination that overprinted mantle-derived $\mu^{182}W$ anomalies. High-$^{3}He/^{4}He$ ratios in
397 the lavas with $\mu^{182}W$ measurements do not necessarily exclude crustal assimilation influence on the Sr-
398 Nd-Pb-W isotopic compositions. For example, a crustally-contaminated Baffin Island lava—sample
399 BI/CS/7—has $^{87}Sr/^{86}Sr_{60}$=0.704912 and $^{143}Nd/^{144}Nd_{60}$=0.512730 compositions consistent with a
400 continental crust contribution, yet the olivines preserve high $^{3}He/^{4}He$ (43.9 Ra) (24). These data suggest
401 that crustal contamination may not impact $^{3}He/^{4}He$ in the same manner it affects the heavy radiogenic
402 isotopic systems, possibly because $^{3}He/^{4}He$ is measured in gas trapped and preserved in olivines formed
403 at depth, prior to significant shallow crustal assimilation that influences the whole rock Sr-Nd-Pb-W
404 isotopic compositions.
405 Significant crustal assimilation appears unlikely in a subset of the BIWG lavas examined in
406 several key studies (23-25). Nonetheless, the extreme enrichment of W in upper continental crust (1.9
407 ppm W) (31) relative to West Greenland lavas (down to 0.022 ppm) (15) suggests that small degrees of
408 continental crust assimilation can dramatically shift $\mu^{182}W$ in the lavas, while leaving the long-lived
409 radiogenic isotopic systems relatively unmodified, as demonstrated in the SI Appendix text. Thus, the
410 presence of $\mu^{182}W$ anomalies in the mantle source of West Greenland lavas cannot be ruled out, since
411 they may have been obscured by small degrees of crustal assimilation. For this reason, $\mu^{182}W$ for the
412 West Greenland picrites are not considered further here nor shown in the figures (see discussion in the SI
413 Appendix, text). The reason the West Greenland lavas are the only modern mantle-derived lavas to plot
414 off the global OIB $\mu^{182}W$-$^{3}He/^{4}He$ array may relate to the fact that they are the only high-$^{3}He/^{4}He$ lavas
415 with $\mu^{182}W$ analyses that erupted in a continental setting, where continental crust assimilation is a
416 concern.
417
418 **Origin of anomalous $\mu^{182}W$ signatures in oceanic hotspots.** The discovery of negative $\mu^{182}W$ values in
419 volcanic hotspot lavas has been interpreted to reflect a geochemical influence from the Earth's core
420 (16,17), which should have low $\mu^{182}W$ (~ -220 (42)). Similarly, ancient high $^{3}He/^{4}He$ has been suggested
421 to reside in Earth's core (24, 47-49). Given the relationship between high $^{3}He/^{4}He$ and anomalous $\mu^{182}W$

in modern OIB, it is tempting to suggest a model where both high $^{3}He/^{4}He$ and anomalous $\mu^{182}W$ are supplied to the mantle by the core. While there are limited high-precision ^{182}W data on MORB (14), such a model could potentially explain why depleted upper mantle does not host clear ^{182}W anomalies, as the geochemically depleted upper mantle is less likely to host a component that came from or interacted with the core than lower mantle domains sampled by upwelling plumes. An advantage of this model is that it can potentially explain our observation that only geochemically depleted lavas have negative $\mu^{182}W$ anomalies and high $^{3}He/^{4}He$, as any W and He emerging from the core will have a proportionally greater impact on the $^{3}He/^{4}He$ and $\mu^{182}W$ compositions of geochemically depleted mantle domains (which have low W and He concentrations) compared to mantle domains overprinted by recycled crust materials (which have high W and He concentrations and therefore are more immune to He and W isotopic signatures from the core). Furthermore, the non-primitive Pb-isotopic composition of lavas with the most anomalous $\mu^{182}W$ compositions suggests that low $\mu^{182}W$ is not due to preservation of an ancient component in the mantle, but instead mixing between a depleted mantle domain and a component with low $\mu^{182}W$ and high $^{3}He/^{4}He$, a process that is consistent with a core contribution to a depleted mantle domain. However, preservation of high $^{3}He/^{4}He$ in the core is controversial, and a lower mantle origin for high $^{3}He/^{4}He$ has also been suggested (8,10,13). Thus, the analysis and modelling proposed here focus on the modern mantle sources and eruptive products of OIB without any assumptions regarding specific mechanisms for the origin of high $^{3}He/^{4}He$ and anomalous $\mu^{182}W$ in the mantle. Looking forward, models invoked to generate negative $\mu^{182}W$ in the silicate Earth—core addition, late accretion, or silicate Earth differentiation (16,17,41,50,51)—must also explain the link between anomalous $\mu^{182}W$ and high $^{3}He/^{4}He$ in geochemically depleted mantle sources of OIB.

Geodynamic implications for high $^{3}He/^{4}He$ and anomalous ^{182}W in the mantle. Under very restrictive conditions—in geochemically depleted mantle domains lacking recycled crust—early Earth high-$^{3}He/^{4}He$ and anomalous $\mu^{182}W$ signatures have survived convective mixing and interaction with subducted crust to be sampled by upwelling mantle plumes and erupted at modern hotspot volcanoes. The geodynamic process of crustal subduction and recycling plays an outsized role in the destruction of both anomalous $\mu^{182}W$ and high $^{3}He/^{4}He$ because W and ^{4}He concentrations in recycled oceanic and continental crust

may be higher than the high-$^{3}He/^{4}He$ mantle (by approximately one to two orders of magnitude, for oceanic and continental crust, respectively; SI Appendix, Dataset S5). Given evidence provided by high $^{3}He/^{4}He$ and anomalous ^{182}W, the Iceland mantle plume, together with a number of other plumes globally, sample mantle domains that are relatively unmodified by crustal recycling.

This geodynamic framework, which relies on the well-established mechanism of crustal subduction and recycling in the mantle, can be used to evaluate the preservation and distribution of ancient isotopic signatures in the mantle. Like anomalous ^{182}W, nucleosynthetic and short-lived radiogenic isotopic anomalies of elements enriched in Earth's crust (31,32) relative to the mantle (52) (e.g., like ^{142}Nd (18), or even nucleosynthetic ^{92}Mo if heterogeneities are detected in the modern mantle (53)) may be expected to survive primarily in geochemically depleted mantle domains least influenced by recycling. Similarly, nucleosynthetic isotopic signatures for ^{100}Ru (54), if found in the modern mantle (53), would be expected to be less impacted by crustal subduction and recycling than W, because Ru is concentrated in the mantle (52) relative to the crust (31). This would also be the case for elements that are concentrated in the crust or atmosphere relative to the mantle, but are not as efficiently subducted into the mantle as W (e.g., ^{129}Xe (55)). Furthermore, preservation of ancient high-$^{3}He/^{4}He$ and anomalous $\mu^{182}W$ signatures in the mantle requires isolation of the high-$^{3}He/^{4}He$ mantle from subducted crust (56). Due to having higher viscosity, which slows convective motions, the deep lower mantle is an ideal location to preserve ancient domains. The Ultra-Low Velocity Zones (ULVZs) may host anomalous $\mu^{182}W$ (16), and the large low shear wave velocity provinces (LLSVPs) are suggested to host high $^{3}He/^{4}He$ (57). If the LLSVPs (58-60) or ULVZs (61) are denser than ambient mantle, and thus more difficult to entrain, the observation that high $^{3}He/^{4}He$ is entrained only by the hottest, most buoyant plumes is more easily explained (62) (Figure S6). Expanded datasets covering a greater geographic range of hotspots with lower buoyancy fluxes will be important for extending these geophysical relationships to $\mu^{182}W$.

Materials and Methods

We present new whole rock Sr-Nd-Hf-Pb-W isotopic and major and trace element data, $^{3}He/^{4}He$ data obtained on olivines and clinopyroxenes (by crushing and fusion), and olivine major element data for a suite of 18 mid-Miocene lavas from northwest Iceland (Vestfirðir) (SI Appendix, Datasets S1, S2, S3, and S7). Vestfirðir sample locations, constraints on sample ages, descriptions, and age corrections for Sr-Nd-

Hf-Pb isotopic compositions are also provided (SI Appendix, Datasets S1, S8, and S9). Additionally, we present new Sr-Nd-Hf-Pb isotopic data (as well as W isotopic data for ERZ sample A24) for five samples from the SIVZ (20.7 to 25.7 Ra), four samples from the ERZ (20.6 to 25.9 Ra), and one NRZ sample from Vaðalda (33.6 Ra) (SI Appendix, Dataset S1 and S3). Protocols for wet chemistry and radiogenic isotopic analyses (Sr-Nd-Hf-Pb) follow standard techniques and were carried out at four different institutions by TIMS (thermal ionization mass spectrometry) or MC-ICP-MS (multi-collector inductively coupled plasma mass spectrometry) following methods detailed in the SI Appendix, Methods: ENS Lyon (Ecole Normale Supérieure de Lyon: Hf and Pb isotopes by MC-ICP-MS), UCSB (University of California, Santa Barbara: Sr and Nd isotopes by TIMS), UNC (University of North Carolina: Sr and Nd isotopes by TIMS), and USC (University of South Carolina: Sr, Nd, Hf, and Pb isotopes by MC-ICP-MS). Methods for analysis of W isotopes at the University of Vienna are provided elsewhere (SI Appendix, Methods). Measurements of He isotopes, carried out at WHOI (Woods Hole Oceanographic Institution), follow standard protocols (SI Appendix, Methods). Whole rock major and trace element analyses were carried out at the Geoanalytical Lab at Washington State University following standard protocols (SI Appendix, Methods). All new data and protocols associated with this work are provided in the SI Appendix.

Acknowledgements. We acknowledge three anonymous reviewers and an anonymous editor for providing important insights; we also acknowledge Tim Elliott and an anonymous reviewer, who provided comments on a prior version of this manuscript. Bill White and Anekantavada inspired the “least modified” concept. We thank David Peate, Graham Pearson, Ed Garnero, Julien Siebert, James Badro, and Jasper Konter for discussion, Andrea Giuliani for comments, Kristján Jónasson and the late Sveinn Jakobsson for assistance with samples, and Josh Curtice for $^{3}He/^{4}He$ analyses. MGJ acknowledges grants from NSF that funded this research: EAR-1900652 and EAR-1624840. SAH acknowledges support from the Icelandic Research Fund (Grant #196139-051) and the University of Iceland Research Fund. AM-P acknowledges FWF grant V659-N29. MDK acknowledges support from WHOI and NSF OCE-1259218 and Joshua Curtice for help in the lab. TWB was partially supported by NSF EAR-1853856.

References

1. A. Zindler, S.R. Hart, Chemical geodynamics. *Annu. Rev. Earth Planet. Sci.* **14**, 493–571 (1986).

2. A.W. Hofmann, W.M. White, Mantle plumes from ancient oceanic crust. *Earth Planet. Sci. Lett.* ***57***, 421-436 (1982).

3. W.M. White, A.W. Hofmann, Sr and Nd isotope geochemistry of oceanic basalts and mantle evolution. *Nature* **296**, 821–825 (1982).

4. S. Pilet, M.B. Baker, E.M. Stolper. Metasomatized lithosphere and the origin of alkaline lavas. *Science* **320**, 916-919 (2008).

5. Y. Weiss, C. Class, S.L. Goldstein, T. Hanyu, Key new pieces of the HIMU puzzle from olivines and diamond inclusions. *Nature* **537**, 666–670 (2016)

6. J. Eisele, M. Sharma, S.J.G. Galer, J. Blichert-Toft, C.W. Devey, A.W. Hofmann, The role of sediment recycling in EM-1 inferred from Os, Pb, Hf, Nd, Sr isotope and trace element systematics of the Pitcairn hotspot. *Earth Planet. Sci. Lett.* **196**, 197-212 (2002) 197-212

7. P.R. Castillo, C. MacIsaac, S. Perry, J.Veizer, Marine carbonates in the mantle source of oceanic basalts: Pb isotopic constraints. *Scientific Reports* **8** (2018). DOI:10.1038/s41598-018-33178-4

8. S.R. Hart, E.H. Hauri, L.A. Oschmann, J.A. Whitehead, Mantle plumes and entrainment: isotopic evidence. *Science* **256**, 517–520 (1992).

9. D.W. Graham, Noble gas isotope geochemistry of midocean ridge and ocean island basalts; characterization of mantle source reservoirs. in *Noble Gases in Geochemistry and Cosmochemistry* Vol. **47** (eds D. Porcelli, C.J. Ballentine, R. Wieler, R.) 247-318 (Rev. Mineral. Geochem., 2002).

10. C. Class, S.L. Goldstein, Evolution of helium isotopes in the Earth's mantle. *Nature* **436**, 1107–1112 (2005).

11. K.A. Farley, J.H. Natland, H. Craig, Binary mixing of enriched and undegassed (primitive?) mantle components (He, Sr, Nd, Pb) in Samoan lavas. *Earth Planet. Sci. Lett* **111**, 183-199 (1992).

12. B.B. Hanan, D.W. Graham, Lead and helium isotope evidence from oceanic basalts for a common deep source of mantle plumes, *Science* **272**, 991-995 (1996).

13. M.D. Kurz, W.J. Jenkins, S.R. Hart, Helium isotopic systematics of oceanic islands and mantle heterogeneity. *Nature* **297**, 43–47 (1982).

14. A. Mundl, M. Touboul, M.G. Jackson, J.M.D. Day, M.D. Kurz, V. Lekic, R.T. Helz, R.J. Walker, Tungsten-182 heterogeneity in modern ocean island basalts. *Science* **356***,* 66-69 (2017).

15. A. Mundl-Petermeier, R.J. Walker, M.G. Jackson, J. Blichert-Toft, M.D. Kurz, S.A. Halldórsson, Temporal evolution of primordial tungsten-182 and $^{3}He/^{4}He$ signatures in the Iceland mantle plume. *Chem. Geol.* **525**, 245-259 (2019).

16. A. Mundl-Petermeier, R.J. Walker, R.A. Fischer, V. Lekic, M.G. Jackson, M.D. Kurz, Anomalous ^{182}W in high $^{3}He/^{4}He$ Ocean Island Basalts: Fingerprints of Earth's core? *Geochim. Cosmochim. Acta* (2020).

17. H. Rizo, D. Andrault**,** N.R. Bennett, M. Humayun, A. Brandon, I. Vlastelic**,** B. Moine**,** a. Poirier, M.A.

543 Bouhifd, D.T. Murphy, ^{182}W evidence for core-mantle interaction in the source of mantle plumes.
544 *Geochem. Persp. Lett.* **11**, 6-11 (2019). doi: 10.7185/geochemlet.1917
545 18. B.J. Peters, R.W. Carlson, J.M.D. Day, M.F. Horan, Hadean silicate differentiation preserved by
546 anomalous ^{142}Nd/^{144}Nd ratios in the Réunion hotspot source. *Nature* **555**, 89–93 (2018).
547 https://doi.org/10.1038/nature25754
548 19. S. Mukhopadhyay, Early differentiation and volatile accretion recorded in deep-mantle neon and
549 xenon. *Nature*. **486**, 101-104 (2012).
550 20. S. Harðardóttir, S.A. Halldórsson, D.E. Hilton, Spatial distribution of helium isotopes in Icelandic
551 geothermal fluids and volcanic materials with implications for location, upwelling and evolution of the
552 Icelandic mantle plume. *Chem. Geol*. **480**, 12–27 (2018).
553 21. D.R. Hilton, K. Grönvold, C.G. Macpherson, P.R. Castillo, Extreme ^{3}He/^{4}He ratios in northwest
554 Iceland: constraining the common component in mantle plumes. *Earth Planet. Sci. Lett.* **173**, 53–60
555 (1999).
556 22. C.G. Macpherson, D.R. Hilton, J.M.D. Day, D. Lowry, K. Grönvold, High-^{3}He/^{4}He, depleted mantle
557 and low-δ^{18}O, recycled oceanic lithosphere in the source of central Iceland magmatism. *Earth Planet. Sci.*
558 *Lett.* **233**, 411– 427 (2005).
559 23. L.N. Willhite, M.G. Jackson, J. Blichert-Toft, I. Bindeman, M.D. Kurz, S.A. Halldórsson,
560 S. Harðardóttir, E. Gazel, A.A. Price, B.L. Byerly, Hot and heterogenous high-^{3}He/^{4}He components: New
561 constraints from proto-Iceland plume lavas from Baffin Island. *Geochem. Geophys. Geosyst.* **20**, (2019).
562 24. N.A. Starkey, F.M. Stuart, R.M. Ellam, J.G. Fitton, S. Basu, L.M. Larsen, Helium isotopes in early
563 Iceland plume picrites: Constraints on the composition of high ^{3}He/^{4}He mantle. *Earth Planet. Sci. Lett.*
564 **277***,* 91–100 (2009).
565 25. D.W. Graham, L.M. Larsen, B.B. Graham, M. Storey, A.K. Pederson, J.E. Lupton, Helium isotope
566 composition of the early Iceland mantle plume inferred from the Tertiary picrites of West Greenland. *Earth*
567 *Planet. Sci. Lett.* **160**, 241–255 (1998).
568 26. F.M. Stuart, S. Lass-Evans, J.G. Fitton, R.M. Ellam, High ^{3}He/^{4}He ratios in picritic basalts from Baffin
569 Island and the role of a mixed reservoir in mantle plumes. *Nature* **424**, 57–59 (2003).

570 27. J.G. Konter, B.B. Hanan, J. Blichert-Toft, A.A.P. Koppers, T. Plank, H. Staudigel, One hundred million
571 years of mantle geochemical history suggest the retiring of mantle plumes is premature. *Earth Planet. Sci.*
572 *Lett.* **275**, 285–295 (2008)
573 28. A.D. Brandon, R.J. Walker, The debate over core–mantle interaction. *Earth Planet. Sci. Lett.* **232**,
574 211–225 (2005).
575 29. O. Nebel, P.Z. Vroon, D.F. Wiggers de Vries, F.E. Jenner, J.A. Mavrogenes, Tungsten isotopes as
576 tracers of core–mantle interactions: The influence of subducted sediments. *Geochim. Cosmochim. Acta*
577 **74**, 751–762 (2010).
578 30. S.R. Hart, A large-scale isotope anomaly in the Southern Hemisphere mantle. *Nature* **309**, 753-757
579 (1984).
580 31. R.L. Rudnick, S. Gao, Composition of the Continental Crust. In *Treatise on Geochemistry* (eds. H.D.
581 Holland, K.K. Turekian) 1–64. (2003). https://doi.org/10.1016/B0-08-043751-1224 6/03016-4
582 32. A. Gale, C.A. Dalton, C.H. Langmuir, Y. Su, The mean composition of ocean ridge basalts. *Geochem.*
583 *Geophys. Geosyst*. **14** (2013) doi:10.1029/2012GC004334
584 33. T.I. Ireland, R. Arevalo Jr., R.J. Walker, W.F. McDonough, Tungsten in Hawaiian picrites: A
585 compositional model for the sources of Hawaiian lavas. Geochim. Cosmochim. Acta **73**, 4517–4530
586 (2009).
587 34. D. Porcelli, C.J. Ballentine, Models for the distribution of terrestrial noble gases and evolution of the
588 atmosphere. *Rev. Mineral. Geochem*. **46**, 411-480 (2002).
589 35. T. Hanyu, I. Kaneoka, The uniform and low $^{3}He/^{4}He$ ratios of HIMU basalts as evidence for their origin
590 as recycled materials. *Nature* **390**, 273-276 (1997).
591 36. M.G. Jackson, S.R. Hart, A.A.P. Koppers, H. Staudigel, J. Konter, J. Blusztajn, M.D. Kurz, J.A
592 Russell, The return of subducted continental crust in Samoan lavas. *Nature* **448**, 684-687 (2007).
593 37. M.G. Jackson, S.R. Hart, J.G. Konter, M.D. Kurz, J. Blusztajn, K. Farley, Helium and lead isotopes
594 reveal the geochemical geometry of the Samoan plume. *Nature* **514**, 355-358 (2014).
595 38. J.G. Fitton, A.D. Saunders, P.D. Kempton, B.S. Hardarson, Does depleted mantle form an intrinsic
596 part of the Iceland plume? *Geochem. Geophys. Geosys*. *4*, 2003. https://doi.org/10.1029/2002GC000424

39. A.C. Kerr, A.D. Saunders, J. Tarney, N.H. Berry, V.L. Hards, Depleted mantle-plume geochemical signature: No paradox for plume theories. *Geology* **23**, 843–846 (1995).

40. B.B. Hanan, J. Blichert-Toft, R. Kingsley, J.-G. Schilling, Depleted Iceland mantle plume geochemical signature: Artifact of multicomponent mixing? *Geochem. Geophys. Geosyst.* 1 (2000). https://doi.org/10.1029/1999GC000009

41. M. Willbold, T. Elliott, S. Moorbath, The tungsten isotopic composition of the Earth's mantle before the terminal bombardment. *Nature* **477**, 195-198 (2011).

42. M. Touboul, I.S. Puchtel, R.J. Walker, ^{182}W Evidence for long-term preservation of early mantle differentiation products. *Science* **335**, 1065 (2012).

43. A. Klügel, K. Galipp, K. Hoernle, F. Hauff, S. Groom, Geochemical and Volcanological Evolution of La Palma, Canary Islands. *J. Pet*. **58**, 1227–1248 (2017).

44. J.M.D. Day, D.R. Hilton, Origin of ^{3}He/^{4}He ratios in HIMU-type basalts constrained from Canary Island lavas. *Earth Planet. Sci. Lett*. **305**, 226-234 (2011).

45. H. Rizo, R.J. Walker, R.W. Carlson, M. Horan, S. Mukhopadhyay, V. Manthos, D. Francis, M.G. Jackson, Preservation of Earth-forming events in the tungsten isotopic composition of modern flood basalts. *Science* 352, 809-812 (2016).

46. T.S. Kruijer, T. Kleine, No ^{182}W excess in the Ontong Java Plateau source. *Chem. Geol*. **485**, 24–31 (2018).

47. C.G. Macpherson, D.R. Hilton, J.M. Sinton, R.J. Poreda, H. Craig, High ^{3}He/^{4}He ratios in the Manus backarc basin: Implications for mantle mixing and the origin of plumes in the western Pacific Ocean. *Geology* **26**, 1007–1010 (1998).

48. D. Porcelli, A.N. Halliday, The core as a possible source of mantle helium. *Earth Planet. Sci. Lett.* **192**, 45-56 (2001).

49. M.A. Bouhifd, A.P. Jephcoat, V.S. Heber, S.P. Kelley, Helium in Earth's early core. *Nat. Geosci.* **6**, 982-986 (2013).

50. I.S. Puchtel, J. Blichert-Toft, M. Touboul, M.F. Horan, R.J. Walker, The coupled ^{182}W-^{142}Nd record of early terrestrial mantle differentiation. *Geochem. Geophys. Geosyst*. **17**, 2168–2193 (2016).

624 51. M. Willbold, S.J. Mojzsis, H.W. Chen, T. Elliott, Tungsten isotope composition of the Acasta Gneiss
625 Complex. *Earth Planet. Sci. Lett.* **419**, 168-177 (2015).
626 52. W.F. McDonough, Compositional model for the Earth's core. In *Treatise on Geochemistry (Second*
627 *Edition)*, 559-577 (eds Holland, H.D., Turekian, K.K.) (2014).
628 53. R.J. Walker, K. Bermingham, J. Liu, I.S. Puchtel, M. Touboul, E.A. Worsham, In search of late-stage
629 planetary building blocks. *Chem. Geol*. **411**, 125-142 (2015).
630 54. M. Fischer-Gödde, B.M. Elfers, C. Münker, K. Szilas, W.D. Maier, N. Messling, T. Morishita, M. Van
631 Kranendonk, H. Smithies, Ruthenium isotope vestige of Earth's pre-late-veneer mantle preserved in
632 Archaean rocks. *Nature* **579**, 240-244 (2020).
633 55. R. Parai, S. Mukhopadhyay, S. Xenon isotopic constraints on the history of volatile
634 recycling into the mantle. Nature 560, 223-227 (2018).
635 56. W.M. White, Isotopes, DUPAL, LLSVPs, and Anekantavada. *Chem. Geol.* **419**, 10–28 (2015).
636 57. C.D. Williams, S. Mukhopadhyay, M.L. Rudolph, B. Romanowicz, Primitive helium is sourced from
637 seismically slow regions in the lowermost mantle. *Geochem. Geophys. Geosyst.* **20**, 4130-4145 (2019).
638 58. B.H. Heyn, C.P. Conrad, R.G. Trønnes, Stabilizing effect of compositional viscosity contrasts on
639 thermochemical piles. Geophys. Res. Lett. (2018). doi:10.1029/2018gl078799
640 59. H.C.P. Lau, J.X. Mitrovica, J.L. Davis, J. Tromp, H.Y. Yang, D. Al-Attar, Tidal tomography constrains
641 Earth's deep-mantle buoyancy. *Nature* **551**, 321-326 (2017).
642 60. J. Trampert, F. Deschamps, J. Resovsky, D. Yuen, Probabilistic tomography maps chemical
643 heterogeneities throughout the lower mantle. *Science* **306**, 853-856 (2004).
644 61. K. Idehara, Structural heterogeneity of an ultra-low-velocity zone beneath the Philippine Islands:
645 Implications for core-mantle chemical interactions induced by massive partial melting at the bottom of the
646 mantle. *Phys. Earth Planet. Int.* **184**, 80–90 (2011). https://doi.org/10.1016/j.pepi.2010.10.014
647 62. M.G. Jackson, J.G. Konter, T.W. Becker, Primordial helium entrained by the hottest mantle plumes.
648 *Nature* **542**, 340–343 (2017). doi:10.1038/nature21023
649 63. R.K. Workman, S.R. Hart, Major and trace element composition of the depleted MORB mantle
650 (DMM). *Earth Planet. Sci. Lett.* **231**, 53-72 (2005).

64. A. Bouvier, J.D. Vervoort, P.J. Patchett, The Lu–Hf and Sm–Nd isotopic composition of CHUR: constraints from unequilibrated chondrites and implications for the bulk composition of terrestrial planets. *Earth Planet. Sci. Lett.* **273**, 48–57 (2008).

65. M.L.G. Tejada, et al. in Origin and Evolution of the Ontong Java Plateau (eds J.G. Fitton, J.J. Mahoney, P.J. Wallace, A.D. Saunders) 133–150 (Geological Society of London Special Publication 229, 2004).

Figure Legends

Figure 1. Mantle tetrahedron showing that most of the highest $^{3}He/^{4}He$ lavas in Iceland, and global hotspots, do not overlap with the common mantle component (shown as ellipsoid (27)). Four different high-$^{3}He/^{4}He$ (> 25 Ra) components in Iceland (Vestfirðir, ERZ, SIVZ, Baffin Island) are shown. The highest $^{3}He/^{4}He$ (> 30 Ra) samples from each global oceanic hotspot with available Sr-Nd-Pb isotopes—Galapagos, Hawaii, Samoa—are also shown (data sources for these additional lavas are in SI Appendix, Figure S4). EM1, EM2, and HIMU apices of the tetrahedron are published elsewhere (27), as is MORB (63), but EM2 extends to more extreme compositions (36) (indicated by arrow). Data for the highest $^{3}He/^{4}He$ lavas with available Sr-Nd-Pb isotopes from the different Iceland high-$^{3}He/^{4}He$ (> 25 Ra) localities are from SI Appendix, Dataset S1; the Baffin Island lava is the highest $^{3}He/^{4}He$ (39.9 Ra) lava that is the least crustally contaminated (23). Measured values are shown for all lavas except for Baffin Island, where both age-corrected [c] and measured compositions are shown: the calculated present-day Baffin Island mantle source is indistinguishable from the measured composition in the figure (see SI Appendix, Figure S4 caption for details of the age correction and present-day source calculation).

Figure 2. Relationships between $^{3}He/^{4}He$, $^{87}Sr/^{86}Sr$, and $^{206}Pb/^{204}Pb$ in Iceland hotspot lavas showing four geochemically distinct high-$^{3}He/^{4}He$ Iceland components (Vestfirðir, ERZ, SIVZ, and Baffin Island). The highest $^{3}He/^{4}He$ lavas from Hawaii, Galapagos, and Samoa also exhibit heterogeneous Sr-Nd-Pb isotopic compositions. Data sources for these lavas are in SI Appendix, Figure S4. Only the least crustally contaminated Baffin Island lavas are shown (23). Measured heavy radiogenic isotopic compositions are shown for all samples except for Baffin Island, where present-day mantle

source values are plotted (23) (see SI Appendix, Figure S4 caption for details of present-day source calculation). For Iceland hotspot lavas, only high-precision Pb isotopic data (MC-ICP-MS and double-spike TIMS) are shown. Upper Panel: The colored symbols represent lavas with $^{3}He/^{4}He > 21$ Ra sampling all known high-$^{3}He/^{4}He$ regions of the Iceland hotspot—ERZ, SIVZ, NRZ (Vaðalda), Vestfirðir, and BIWG—and white symbols represent Iceland lavas (all of which have $^{3}He/^{4}He < 21$ Ra) from the other regions of Iceland. Lower Panel: Colored symbols represent lavas with $^{3}He/^{4}He > 21$ Ra sampling all known high-$^{3}He/^{4}He$ regions of the Iceland hotspot, and the white symbols represent Iceland lavas with $^{3}He/^{4}He \leq 21$ Ra (or lavas that have not been characterized for $^{3}He/^{4}He$).

Figure 3. Relationships between $^{3}He/^{4}He$, $\mu^{182}W$, $^{143}Nd/^{144}Nd$, and $^{206}Pb/^{204}Pb$ in global OIB showing that only geochemically-depleted OIB (i.e., high $^{143}Nd/^{144}Nd$ and low $^{206}Pb/^{204}Pb$) lacking recycled crust signatures host the highest $^{3}He/^{4}He$ and largest magnitude $\mu^{182}W$ anomalies. The compilation of He-Sr-Nd-Pb isotopes (from this study and prior studies; SI Appendix, Dataset S4) for lavas with available $\mu^{182}W$ shows that only lavas with low $^{206}Pb/^{204}Pb$ (top panel) or high $^{143}Nd/^{144}Nd$ (middle panel) host the most extreme negative $\mu^{182}W$ anomalies. Lavas with the most extreme negative $\mu^{182}W$ anomalies also exhibit high $^{3}He/^{4}He$ (bottom panel, where only lavas with available $\mu^{182}W$ data are shown). In contrast, the mantle endmembers EM1, EM2, and HIMU have low $^{3}He/^{4}He$ and lack anomalous $\mu^{182}W$, as does DM. The chondritic reference $^{143}Nd/^{144}Nd$ is published elsewhere (64). All data and error bars (2σ) are provided in SI Appendix, Dataset S4. The $^{143}Nd/^{144}Nd$ and $^{206}Pb/^{204}Pb$ for Ontong Java Plateau (OJP) is an average of Kroenke- and Kwaimbaita-type lavas (65); present-day mantle source compositions (23) are show in lieu of measured or age-corrected ages due to the 120 Ma eruption age. The OJP $\mu^{182}W$ data shown lack of anomalous signatures (41,46).

Figure 4. Impact of mixing subducted crust and depleted mantle (DM) on OIB mantle domains with high-$^{3}He/^{4}He$ and anomalous $\mu^{182}W$ compositions. The mixing models demonstrate how subducted crustal materials, and DM, reduce $^{3}He/^{4}He$ and overprints resolvable $\mu^{182}W$ anomalies in the mantle, thereby generating the negatively sloping OIB array. Sediment (large grey box), oceanic crust (large grey triangle), and depleted mantle (DM, large black box) are each mixed with four OIB mantle sources with

high $^{3}He/^{4}He$ and anomalous $\mu^{182}W$. Endmember compositions used are in SI Appendix, Dataset S5. Samoa and Hawaii have indistinguishable trends (14-16), but Samoan $\mu^{182}W$ is characterized to higher $^{3}He/^{4}He$. Intervals are marked at 10% for mixtures with DM; for mixtures with sediment and oceanic crust, intervals are marked at 1% for the first 10% addition of subducted material, thereafter every 20%. Sediment (derived from continental crust) and oceanic crust generate compositions similar to the extreme Samoan EM2 lava (5% subducted sediment), the extreme Pitcairn EM1 lava (3% sediment), and the extreme Mangaia HIMU lavas (25% oceanic crust) (see SI Appendix, Datasets S4 and S5). OIB data symbols are the same as in Figure 3. Symbols are the same as in Figure 3; OIB data symbols and error bars (2σ) are provided in SI Appendix, Dataset S4.

Figure 5. $\mu^{182}W$ as a function of $D^{Sr\text{-}Nd\text{-}Pb}$ showing that OIB sampling significant recycled crust (represented by extreme EM1, EM2, and HIMU lavas), or MORB, lack $\mu^{182}W$ anomalies. Left panel: Samples with the lowest $D^{Sr\text{-}Nd\text{-}Pb}$ (defined in main text) have the smallest contributions from the EM1, EM2, and HIMU mantle endmembers (and the smallest recycled crust contributions). Samples with the highest $D^{Sr\text{-}Nd\text{-}Pb}$ plot closest to EM1, EM2, and HIMU in Sr-Nd-Pb isotopic space (and host the greatest recycled crust contributions). Binary mixing lines are shown between a melt with anomalous $\mu^{182}W$ and melts of EM1 (blue line), EM2 (pink line), HIMU (purple line), and MORB melts of DM (black mixing line) (see SI Appendix, Dataset S6 for model compositions); 10% mixing increments are shown. Symbols are the same as Figure 3 and data (and 2σ errors) are from SI Appendix Dataset S4 (except for OJP data, which are indicated in Figure 3). Right panel: Illustrates calculation of $D^{Sr\text{-}Nd\text{-}Pb}$ values and shows examples of three large $D^{Sr\text{-}Nd\text{-}Pb}$ values, one medium $D^{Sr\text{-}Nd\text{-}Pb}$ value, and one small $D^{Sr\text{-}Nd\text{-}Pb}$ value; all $D^{Sr\text{-}Nd\text{-}Pb}$ values are distances in $^{87}Sr/^{86}Sr$-$^{143}Nd/^{144}Nd$-$^{206}Pb/^{204}Pb$ isotope space calculated between the depleted reference composition (Depl. Ref. Comp.) and OIB samples.

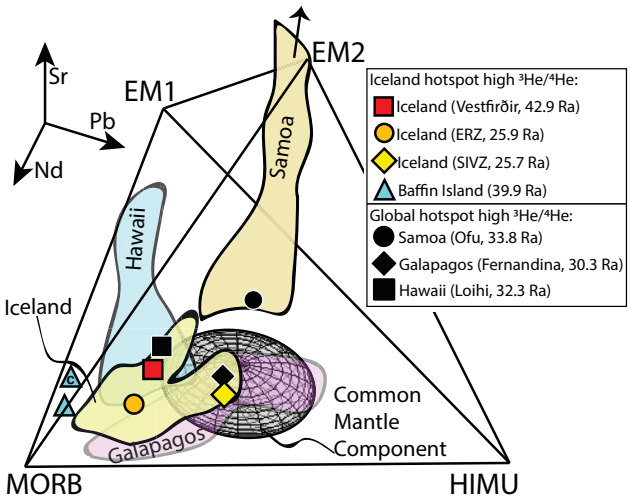
Sr
Pb
Nd
EM1
EM2
Samoa
Hawaii
Iceland
Galapagos
Common
Mantle
Component
MORB
HIMU
Iceland hotspot high ³He/⁴He:
Iceland (Vestfirðir, 42.9 Ra)
Iceland (ERZ, 25.9 Ra)
Iceland (SIVZ, 25.7 Ra)
Baffin Island (39.9 Ra)
Global hotspot high ³He/⁴He:
Samoa (Ofu, 33.8 Ra)
Galapagos (Fernandina, 30.3 Ra)
Hawaii (Loihi, 32.3 Ra)

Figure 1

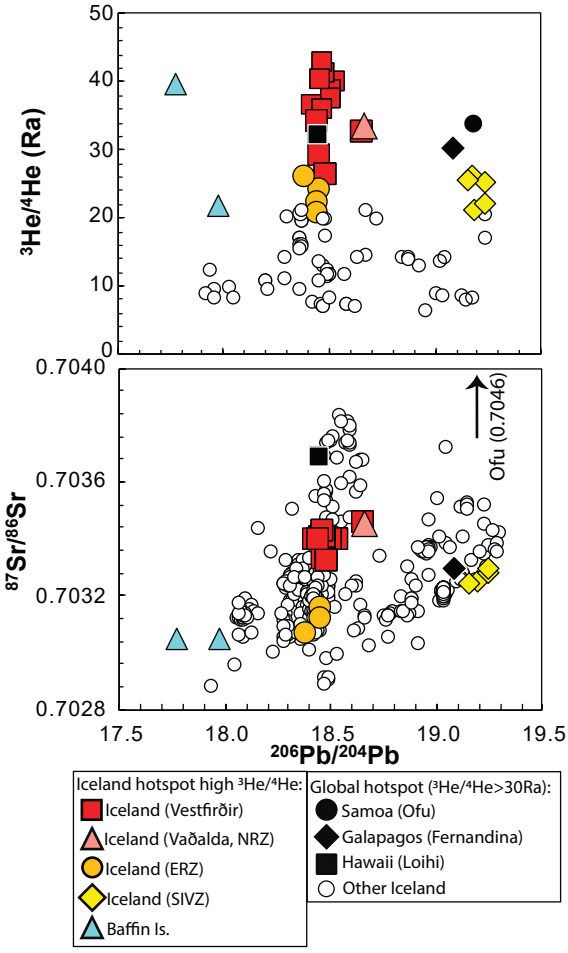
50
40
30
20
10
0
$^{3}He/^{4}He$ (Ra)
0.7040
0.7036
0.7032
0.7028
$^{87}Sr/^{86}Sr$
Ofu (0.7046)
17.5
18.0
18.5
19.0
19.5
$^{206}Pb/^{204}Pb$
Iceland hotspot high $^{3}He/^{4}He$:
Iceland (Vestfirðir)
Iceland (Vaðalda, NRZ)
Iceland (ERZ)
Iceland (SIVZ)
Baffin Is.
Global hotspot ($^{3}He/^{4}He$>30Ra):
Samoa (Ofu)
Galapagos (Fernandina)
Hawaii (Loihi)
Other Iceland

Figure 2

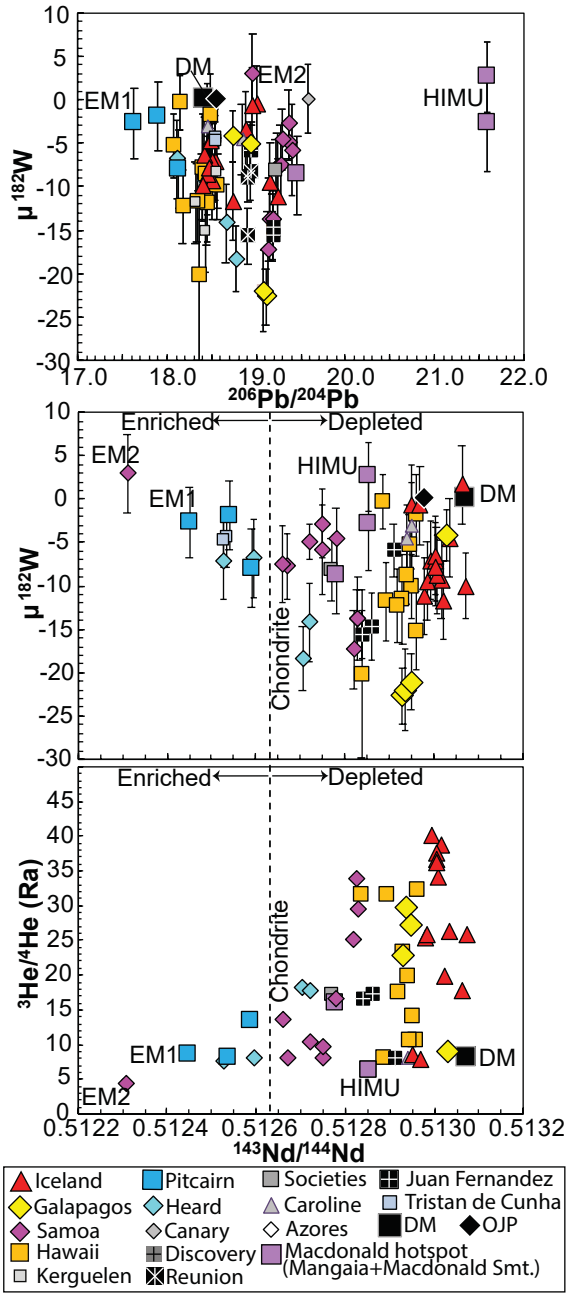
DM
EM2
EM1
HIMU
μ182W
206Pb/204Pb
Enriched
Depleted
Chondrite
3He/4He (Ra)
143Nd/144Nd
Iceland
Pitcairn
Societies
Juan Fernandez
Galapagos
Heard
Caroline
Tristan de Cunha
Samoa
Canary
Azores
DM
OJP
Hawaii
Discovery
Macdonald hotspot (Mangaia+Macdonald Smt.)
Kerguelen
Reunion

Figure 3

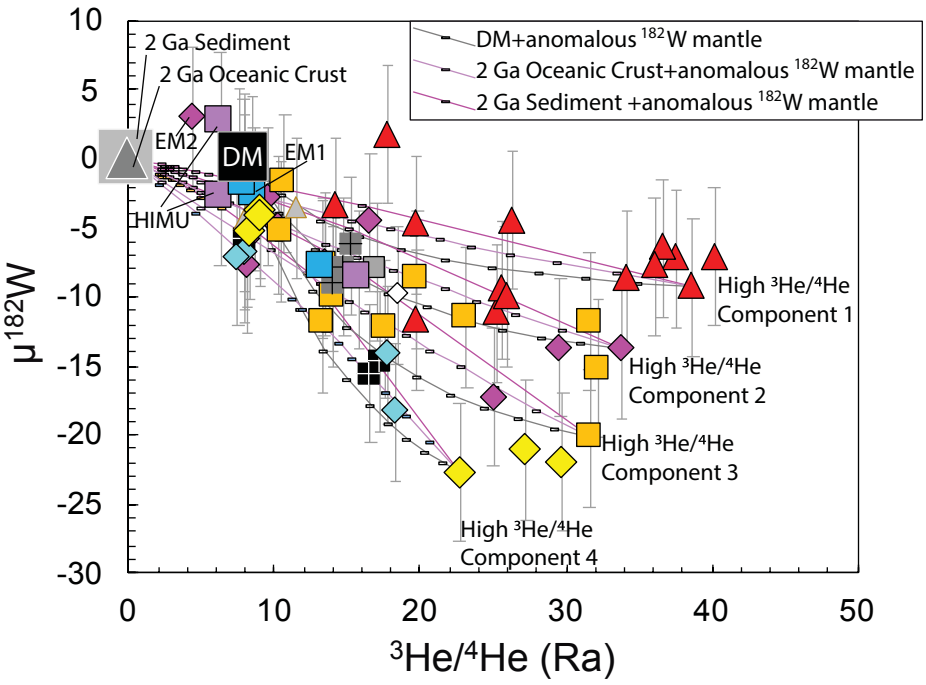
DM+anomalous 182W mantle
2 Ga Oceanic Crust+anomalous 182W mantle
2 Ga Sediment +anomalous 182W mantle
2 Ga Sediment
2 Ga Oceanic Crust
EM2
DM
EM1
HIMU
High 3He/4He Component 1
High 3He/4He Component 2
High 3He/4He Component 3
High 3He/4He Component 4
μ182W
3He/4He (Ra)
10
5
0
-5
-10
-15
-20
-25
-30
0
10
20
30
40
50

Figure 4

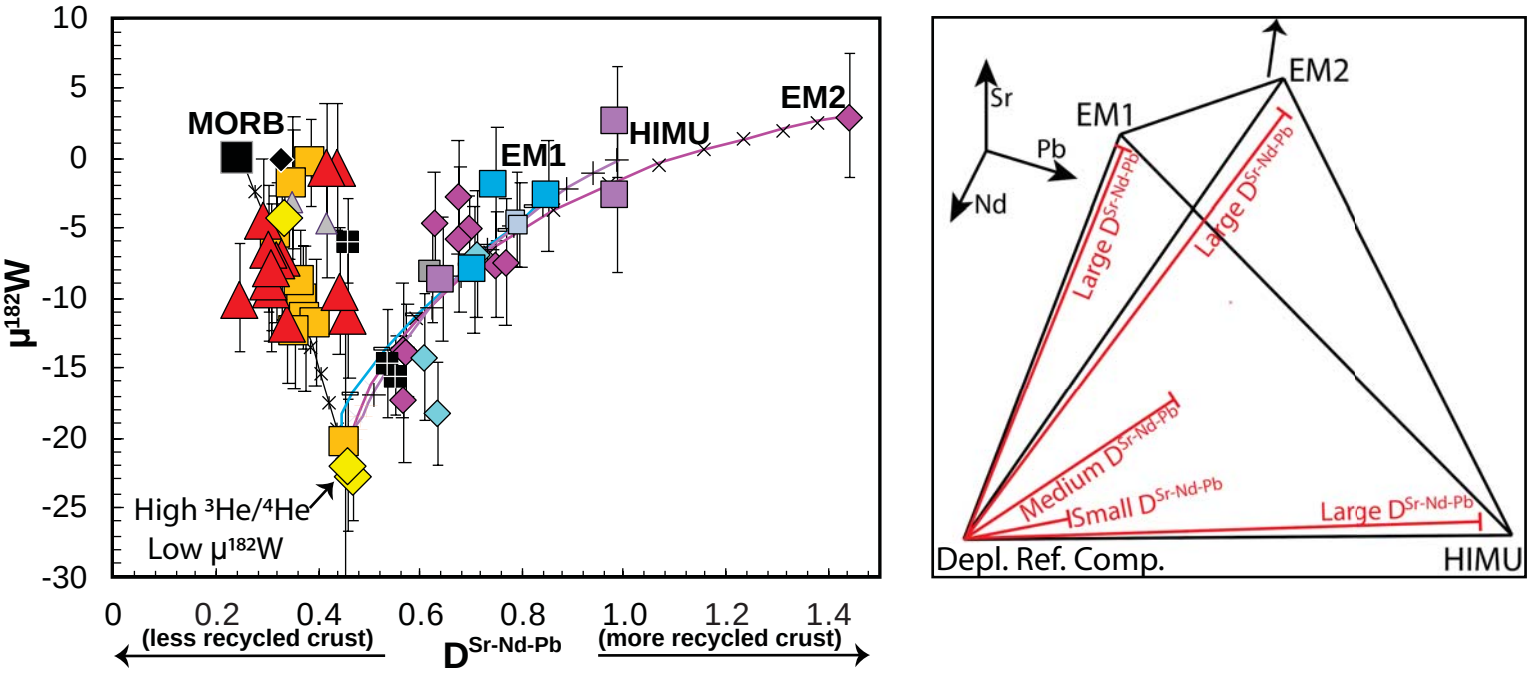
10
5
0
-5
-10
-15
-20
-25
-30
μ182W
MORB
EM1
HIMU
EM2
High 3He/4He
Low μ182W
0
0.2
0.4
0.6
0.8
1.0
1.2
1.4
(less recycled crust)
DSr-Nd-Pb
(more recycled crust)
Sr
Pb
Nd
EM1
EM2
Large DSr-Nd-Pb
Large DSr-Nd-Pb
Medium DSr-Nd-Pb
Small DSr-Nd-Pb
Large DSr-Nd-Pb
Depl. Ref. Comp.
HIMU

Figure 5